Astronomy & Astrophysics

Where intermediate-mass black holes could hide in the Galactic Centre

A full parameter study with the S2 orbit

GRAVITY Collaboration[*]: O. Straub[1,2,**], M. Bauböck[3,1], R. Abuter[4], N. Aimar[5], P. Amaro Seoane[19,1,20],
A. Amorim[6,7], J. P. Berger[8,4], H. Bonnet[4], G. Bourdarot[1], W. Brandner[9], V. Cardoso[7,22], Y. Clénet[5], Y. Dallilar[1],
R. Davies[1], P. T. de Zeeuw, J. Dexter[11], A. Drescher[1], F. Eisenhauer[1], N. M. Förster Schreiber[1], A. Foschi[7,10],
P. Garcia[12,7], F. Gao[13,1], E. Gendron[5], R. Genzel[1,14], S. Gillessen[1], M. Habibi[1], X. Haubois[15], G. Heißel[21,5],
T. Henning[9], S. Hippler[9], M. Horrobin[17], L. Jochum[15], L. Jocou[8], A. Kaufer[15], P. Kervella[5], S. Lacour[5],
V. Lapeyrère[5], J.-B. Le Bouquin[8], P. Léna[5], D. Lutz[1], T. Ott[1], T. Paumard[5], K. Perraut[8], G. Perrin[5], O. Pfuhl[4,1],
S. Rabien[1], D. C. Ribeiro[1], M. Sadun Bordoni[1], S. Scheithauer[9], J. Shangguan[1], T. Shimizu[1], J. Stadler[16,1],
C. Straubmeier[17], E. Sturm[1], L. J. Tacconi[1], F. Vincent[5], S. von Fellenberg[18,1], F. Widmann[1], E. Wieprecht[1],
E. Wiezorrek[1], and J. Woillez[4]

(Affiliations can be found after the references)

ABSTRACT

Context. In the Milky Way the central massive black hole, Sgr A*, coexists with a compact nuclear star cluster that contains a sub-parsec concentration of fast-moving young stars called S-stars. Their location and age are not easily explained by current star formation models, and in several scenarios the presence of an intermediate-mass black hole (IMBH) has been invoked.
Aims. We use GRAVITY astrometric and SINFONI, KECK, and GNIRS spectroscopic data of S2, the best known S-star, to investigate whether a second massive object could be present deep in the Galactic Centre (GC) in the form of an IMBH binary companion to Sgr A*.
Methods. To solve the three-body problem, we used a post-Newtonian framework and consider two types of settings: (i) a hierarchical set-up where the star S2 orbits the Sgr A*–IMBH binary and (ii) a non-hierarchical set-up where the IMBH trajectory lies outside the S2 orbit. In both cases we explore the full 20-dimensional parameter space by employing a Bayesian dynamic nested sampling method.
Results. For the hierarchical case we find the strongest constraints: IMBH masses $>2000\,M_\odot$ on orbits with smaller semi-major axes than S2 are largely excluded. For the non-hierarchical case, the chaotic nature of the problem becomes significant: the parameter space contains several pockets of valid IMBH solutions. However, a closer analysis of their impact on the resident stars reveals that IMBHs on semi-major axes larger than S2 tend to disrupt the S-star cluster in less than a million years. This makes the existence of an IMBH among the S-stars highly unlikely.
Conclusions. The current S2 data do not formally require the presence of an IMBH. If an IMBH hides in the GC, it has to be either a low-mass IMBH inside the S2 orbit that moves on a short and significantly inclined trajectory or an IMBH with a semi-major axis $>1''$. We provide the parameter maps of valid IMBH solutions in the GC and discuss the general structure of our results and how future observations can help to put even stronger constraints on the properties of IMBHs in the GC.

Key words. black hole physics – gravitation – Galaxy: center – Galaxy: nucleus – Galaxy: kinematics and dynamics – Galaxy: structure

1. Introduction

The nuclear star cluster in the Milky Way can, due to its proximity to Earth (R_0 = 8.28 kpc, GRAVITY Collaboration 2019, 2021; Do et al. 2019), be resolved into individual stars. In its entirety, it has an oblate shape and extends in the K-band to about $178''$ (i.e. 7.2 pc at R_0, Becklin & Neugebauer 1968; Schödel et al. 2014; Fritz et al. 2016) around the central massive black hole, Sagittarius A^* (Sgr A*, Eckart & Genzel 1996; Ghez et al. 1998, 2008; Schödel et al. 2002; GRAVITY Collaboration 2018) and consists predominantly of old and evolved stars. However, in its innermost region,

the central $12''$ (0.5 pc), it contains a dense and diverse population of stars with a surprising accumulation of young and massive O and B stars. They are found in the stellar disc of WR/O stars that extends from $0.8''$ to $12''$ and shows a clockwise motion (Paumard et al. 2006; Bartko et al. 2009, 2010; Lu et al. 2009; Yelda et al. 2014), and in the S-star cluster that resides inside the disc's truncation radius and can have ages as young as $3-15 \times 10^6$ years (Ghez et al. 2003; Eisenhauer et al. 2005; Pfuhl et al. 2011; Lu et al. 2013; Habibi et al. 2017; von Fellenberg et al. 2022).

Accompanying the morphology of the Galactic core region are two puzzling observations. On the one hand, there are the isotropically oriented orbital planes and the approximately thermal distribution of the orbital eccentricities of the S-stars. With only a few million years of age, the early B-type stars thus appear too young to be that thermally relaxed in such close proximity to Sgr A* (the paradox of youth; Ghez et al. 2003). On the

other hand, in dynamically relaxed systems, one would expect mass segregation where more massive bodies like the WR/O stars are located closer to the centre than the less massive S-stars (Alexander & Hopman 2009).

Over the past decades, many models have been proposed to explain the age and location of the S-stars. Hansen & Milosavljević (2003) were the first to suggest that an intermediate-mass black hole (IMBH) is present in the Galactic Centre (GC). They argue that an IMBH could have dragged the S-stars from a greater, more star formation friendly distance inwards. However, the telltale trail of young stars outside 0.5 pc, which would support a collective inward migration of such a cluster, is not observed (Feldmeier-Krause et al. 2015). Nonetheless, the idea that an IMBH is associated with the location and the distribution of orbital elements of the S-star has been picked up in a variety of studies, and is still a matter of debate today.

Not all scenarios require an IMBH, though. Chen & Amaro-Seoane (2014, 2015) resolve the paradox of youth and mass segregation problem with a rapid redistribution of stellar orbits based on a Kozai-Lidov-like resonance induced by a stellar disc that was more massive and extended in the past. Generozov & Madigan (2020) argue that if the S-stars are sourced by the WR/O disc via the Hills mechanism (stellar binary disruption by a massive third body; Hills 1988), an additional relaxation mechanism is needed to reproduce their present-day distribution on the short timescale given by their ages. They conclude that within a few million years either scalar resonant relaxation from the observed isotropic star cluster or an IMBH of $\sim 10^3 M_\odot$ at 250 mas could achieve the observed eccentricities. Employing a cluster of stellar black holes (SBHs) as relaxation agent, Perets et al. (2009) found in N-body simulations running over 20 Myr that a thermal eccentricity distribution is a natural consequence of random gravitational encounters of stars with a population of SBHs with a total mass of $\propto 10^4 M_\odot$ in the inner 0.1 pc. Assuming a cluster of more massive SBHs, Tep et al. (2021) arrive at the same conclusion, but on a shorter timescale. This is consistent with the upper limit on the dark mass distribution of about 15 000 $M_\odot$ within 0.1–0.2 pc derived by GRAVITY Collaboration (2022).

The paper is structured as follows. Sections 2 and 3 discuss whether or not it is realistic to expect an IMBH in the GC and what constraints on its mass and location have been found in previous studies. In Sect. 4 we describe the data set used, and in Sect. 5 we present the model and methodology we used to fit them. Our results follow in Sect. 6. In Sect. 7 we discuss the stability analysis. Finally, in Sect. 8 we add concluding remarks and an outlook on the future.

2. Possibility of IMBHs in the Galactic Centre

Theoretically, black holes can have any mass upwards of the Planck mass[1] Astrophysical black holes, however, essentially only come in two 'flavours'.

The first is stellar black holes, with masses ranging from about 3–100 $M_\odot$, where $M_\odot = 2 \times 10^{33}$ g, which form via gravitational collapse of massive stars that depleted their nuclear energy source (e.g. Oppenheimer & Snyder 1939; Penrose 1965; Mirabel 2017).

The second flavour is massive black holes (MBHs), with masses higher than $10^6 M_\odot$, which are thought to form via direct

or indirect gravitational collapse of an initial massive gas cloud and to co-evolve symbiotically with their host galaxies (e.g. Rees 1978). Although there is an emerging consensus regarding the growth of supermassive BHs thanks to Sołtan's argument (Sołtan 1982), the evolution of MBHs with masses up to $10^7 M_\odot$, such as our own MBH in the Galactic Centre (with a mass of $\sim 4.2 \times 10^6 M_\odot$), is enigmatic.

There is compelling evidence for the existence of SBHs from both electromagnetic observations (e.g. Narayan & McClintock 2013; Casares & Jonker 2014; Corral-Santana et al. 2016) and gravitational wave detection (Abbott et al. 2021). Equally well established is the occurrence of MBHs at the centres of massive galaxies (e.g. Magorrian et al. 1998; Volonteri 2010; Kormendy & Ho 2013). Moreover, the increasing number of observations of luminous quasars at very high redshift indicates that some supermassive BHs with masses $>10^8 M_\odot$ already existed when the Universe was less than a billion years old (Mortlock et al. 2011; Wu et al. 2015; Bañados et al. 2018; Yang et al. 2020).

Intermediate-mass black holes are thought to bridge the gap between these two BH populations and, more importantly, to be the building blocks in the formation process of MBHs. Understanding them is crucial to answering the question of how the young and supermassive quasars could develop into behemoths on such short timescales.

The following three MBH formation channels predict the appearance of IMBHs at different times and in different numbers. There are two early formation mechanisms that rely on the properties of zero-metallicity gas and can therefore only operate at redshift $z > 10$. In the young Universe, the pristine hydrogen gas could have either coagulated into the first generation of massive Population III stars (Madau & Rees 2001) or it could have contracted uniformly to directly form a single supermassive star that then collapsed into an intermediate-mass seed BH (Loeb & Rasio 1994; Begelman et al. 2006), possibly via an accreting quasi-star phase (Hoyle & Fowler 1963; Begelman 2010; Wise et al. 2019). The inefficient cooling due to the presence of primordial hydrogen inhibits premature fragmentation and pair-instability supernovae such that the Population III stars and the supermassive star could have reached masses significantly higher than 100 $M_\odot$ and lead to early intermediate-mass seed BHs (Ohkubo et al. 2009).

Quite distinct from the two early seeding mechanisms is the third dynamical formation channel where gravitational runaway and hierarchical black hole mergers in dense nuclear star clusters can form many IMBH kernels (Quinlan & Shapiro 1990; Portegies Zwart & McMillan 2002; Freitag et al. 2006; Stone et al. 2017). Antonini et al. (2019) have calculated that IMBHs can indeed form via hierarchical mergers in star clusters with high enough escape velocities and densities. Rizzuto et al. (2021) have pointed out that IMBHs could form in $\lesssim 15$ Myr, in particular in young and compact star clusters. While the two early seeding mechanisms produce at most one IMBH per galaxy halo at high redshift, this latter process can operate throughout cosmic time and could provide a channel to create an IMBH in any dense stellar system (for comprehensive reviews, see Miller & Colbert 2004; Mezcua 2017; Greene et al. 2020). Recently, a mass-gap SBH (or low-mass IMBH) of around 150 $M_\odot$ has been identified as the product of a coalescence of two SBHs via gravitational wave detection (GW190521, Abbott et al. 2020a,b; Nitz & Capano 2021), supporting scenarios with dynamical hierarchical mergers.

Today, intermediate-mass black holes that formed via the early seeding processes are thus expected to populate

---

[1] $m_P = (\frac{\hbar c}{G})^{1/2} = 2.2 \times 10^{-5}$ g.

the centres of low-mass dwarf[2] and satellite galaxies (e.g. Mezcua et al. 2016, 2018), whereas IMBHs formed via dynamical mergers are thought to be found rather in globular clusters (Miller & Hamilton 2002; Baumgardt et al. 2005) and nuclear star clusters (Miller & Lauburg 2009; Neumayer et al. 2020). The most convincing IMBH candidates are indeed found in low-mass galaxies and have masses $10^4 \lesssim M < 10^6 \, M_\odot$, for example HLX-1 (Farrell et al. 2009; Webb et al. 2017) and the Large Magellanic Cloud (LMC, Erkal et al. 2019). During their evolution, galaxies may accrete nearby satellite or dwarf galaxies, which could deposit a substantial number of wandering IMBHs, each surrounded by a stellar system, in the galactic halos (e.g. the Milky Way, Rashkov & Madau 2014). Moreover, centres of galaxies have in principle deep enough potential wells to retain SBH merger products in their nuclear star clusters (see Hailey et al. 2018; Fragione et al. 2022; Rose et al. 2022). Therefore, it seems conceivable that the centre of the Milky Way could host an IMBH. Although the question arises of whether it could hide among the S-stars.

3. Constraints on IMBH mass and location in the Galactic Centre

The first constraints on the mass and location of an IMBH in the GC came from a study of dynamical processes that can eject hyper-velocity stars from the GC at average speeds of $400-2000 \, \mathrm{km \, s^{-1}}$ (Yu & Tremaine 2003) and the measurement of the proper motion of Sgr A* that is consistent with no acceleration (Reid & Brunthaler 2004, 2020). These studies exclude in essence IMBH masses of $M \gtrsim 3 \times 10^4 \, M_\odot$ within the S-star cluster and the WR/O disc.

Merritt et al. (2009) employed long-term N-body simulations to show that the presence of an IMBH can randomise the orbital planes of 19 S-stars in one million years if the IMBH mass exceeds $1500 \, M_\odot$ and its pericentre distance is smaller than 250 mas. N-body simulations of the orbits of S-stars around Sgr A* in the presence of an IMBH have been used to study the effects of an IMBH on the orbit of S2 in particular. These codes typically solve the N-body problem numerically (e.g. with a post-Newtonian approximation[3]) up to order 2.5 and with 21 S-stars in addition to the MBH and the IMBH (Gualandris & Merritt 2009; Gualandris et al. 2010).

Many-body systems are chaotic in nature, and in order to make the orbital fitting procedure manageable the N-body codes traditionally rely on a discrete but serviceable set of reasonable IMBH orbital parameters, for instance three different eccentricity values paired with a range of interesting IMBH masses and a fixed set of inclinations and orbital angles. Another way to tackle the chaotic nature of the three-body problem is used by Naoz et al. (2020) who studied a high-order analytic approximation of the inverse Kozai-Lidov equations. Considering the stability of the S2 orbit, they could rule out a $10^5 \, M_\odot$ companion on a circular orbit with a semi-major axis greater than 20 mas.

In GRAVITY Collaboration (2020) we collected the available constraints on the IMBH mass and semi-major axis in the literature and presented them together with an estimate of the

constraints that could be achieved by the GRAVITY instrument. In this work we show the actual IMBH constraints based on GRAVITY (and SINFONI/KECK/GNIRS) data of S2. In terms of simulation and fitting technique, in this work we go a step further than previous N-body simulations and explore not only a few selected sets of IMBH orbits, but the full-dimensional parameter space. In this way we obtain the most realistic constraints based on current high angular resolution interferometric and spectroscopic infrared observations.

4. Data

The star S2 moves on a highly elliptical 16-year orbit around Sgr A* and has been monitored since 1992. The resulting high-precision data of nearly 2.5 orbits have not only lead to the direct measurement of the compact mass in the GC, $M_0 \approx 4.30 \times 10^6 \, M_\odot$, and its distance, $R_0 \approx 8.28 \, \mathrm{kpc}$ (GRAVITY Collaboration 2019, 2022), but have also delivered evidence for relativistic effects such as the gravitational redshift (GRAVITY Collaboration 2018; Do et al. 2019) and the Schwarzschild precession (GRAVITY Collaboration 2020), as well as the local position invariance (Amorim et al. 2019).

In this work, we use the astrometry data taken from 2017–2021 by the GRAVITY beam combiner, a K-band infrared interferometer at the European Southern Observatory's Very Large Telescope (ESO's VLT) together with spectroscopic data collected from 2000–2021 by NIRC2 at the Keck Observatory, SINFONI at the VLT, and GNIRS at the Gemini Observatory (see GRAVITY Collaboration 2022, for a more detailed description).

All GRAVITY data have been recorded in low resolution and split (linear) polarisation. Each exposure consists of a total integration time of 320 s, comprised of 32 consecutive frames every 10 s. One VLT observation block contains two different targets, the star S2 and the black hole Sgr A*. During the pericentre passage of S2 from 2017 to 2018, both objects were detected simultaneously in the same fibre field of view (FoV = 60 mas). In all epochs from 2019 onwards, the separation between S2 and Sgr A* has been larger than the FoV and the objects have been targeted individually. In this dual-beam mode we first take an exposure with the fibre centred on S2 and then dither to Sgr A* and take a sequence of four exposures. We repeat this 1+4 pattern throughout the available night. We then use the latest version of the standard GRAVITY data reduction pipeline to reduce all data. The interferometric observables, the closure phase and visibility, of the star S2 are consistent with a single point source such that we can use it as a phase reference to calibrate the Sgr A* exposures. In this way we can calculate the separation vector between S2 and Sgr A* from the fitted phase offsets (see Appendix A in GRAVITY Collaboration 2022). The resulting GRAVITY astrometry has a root mean square (rms) uncertainty of $\approx 50 \, \mu\mathrm{as}$; SINFONI and KECK – GNIRS data have a rms uncertainty of $\approx 12 \, \mathrm{km \, s^{-1}}$ and $\approx 45 \, \mathrm{km \, s^{-1}}$, respectively.

In this work, we are not using any adaptive optics (AO) astrometric data collected by NACO/VLT. The reason we omit about 75 a priori perfectly valid AO imaging measurements between 2003 and 2019 is that the calibration of the reference frame between NACO and GRAVITY is largely degenerate with adding an IMBH. In sampling such a posterior, the solutions run away towards an arbitrary calibration factor and arbitrarily high IMBH masses. We avoid the problem by excluding the AO measurements and using only the GRAVITY high-resolution interferometric astrometry, which is internally self-consistent and of

---

[2] Some dwarf galaxies can have surprisingly massive central BHs (e.g. Bustamante-Rosell et al. 2021), possibly due to dynamical mergers of IMBHs in complexes of young stellar clusters (Amaro-Seoane et al. 2014).

[3] The post-Newtonian approximation is a method for solving Einstein's field equations by expanding them in terms of a small parameter $\epsilon \sim (v/c)^2$.

a much higher precision than the NACO data (rms of about 1.7 mas).

5. Methodology

We consider two scenarios. In the hierarchical set-up, Sgr A* has a close IMBH binary companion with a small semi-major axis $0.01'' \leq a_i \leq 0.1''$. The star S2 with $a = 0.125''$ orbits around this binary's centre of mass. The IMBH orbit lies in this case inside the S2 orbit. In the non-hierarchical set-up the IMBH has a semi-major axis $0.1'' \leq a_i \leq 1''$, which crosses the S2 orbit or lies entirely outside of the S2 orbit but still within the S-star cluster. In this set-up the centre of mass is Sgr A*. We treat these two distinct cases separately.

5.1. Orbital integration

To simulate the orbits of a three-body system consisting of Sgr A*, the star S2, and an IMBH, we adapted the publicly available REBOUND N-body code (Rein & Liu 2012). We used REBOUND in combination with the REBOUNDx package (Tamayo et al. 2020) which incorporates the first-order post-Newtonian effects from all massive bodies in the system. The simulations were integrated using a 15th order Gauss-Radau integrator (IAS15; Rein & Spiegel 2015).

We first add Sgr A* at the origin of the coordinate system. In order to minimise the error introduced to the S2 orbital parameters due to the transformation between a flat Cartesian coordinate system and the relativistic spacetime around the black hole, we add the star S2 near the apocentre of its orbit (i.e. we set the initial timestamp of the osculating Keplerian orbit to $t_0 = 2010.0$). We then integrate the orbit forward to the date of the last GRAVITY observation used in this work: $t = 2021.570283$. Here we convert the orbital elements of S2 (a_{S2}, e_{S2}, i_{S2}, Ω_{S2}, ω_{S2}, $T_{\mathrm{peri,S2}}$) into a state vector consisting of the position and velocity. This ensures the correct starting position with regard to the observational data. We then remove the star S2 and add the IMBH, and redefine the coordinate system so that the origin is now at the centre of mass. Finally, we add the star S2 with the starting position and velocity vectors calculated previously.

Once we have initialised the simulation, we integrate the orbits of all three masses backwards in time to the earliest velocity data point, at $t = 2000.476$. Given the larger uncertainties of the early data points, we integrate backwards in time to make sure S2 is on the correct orbit in the present day. We take into account the Rømer delay arising from the change in the light travel time at various points along the S2 orbit. We approximate the delay following GRAVITY Collaboration (2018) as

$$t_{\mathrm{em}} = t_{\mathrm{obs}} - \frac{z(t_{\mathrm{obs}})}{c}\left(1 - \frac{v_z(t_{\mathrm{obs}})}{c}\right), \qquad (1)$$

where t_{em} is the time at which a photon is emitted, t_{obs} is the time at which it is observed, and z and v_z represent the line-of-sight distance and velocity, respectively. For each observation we therefore first calculate the position and velocity at the observed time and then use these values to approximate the emitted time. We then integrate the orbit of S2 to $t = t_{\mathrm{em}}$ to compare with the data.

The REBOUNDx module includes general relativistic effects up to first order in the post-Newtonian approximation in the calculation of the orbits of all three masses, but it does not account for the relativistic effects experienced by the photons emitted by those masses. We therefore explicitly account for the transverse

Doppler shift and the gravitational redshift for the star S2 when calculating the observed radial velocity. Specifically, we assume a Schwarzschild geometry for the MBH Sgr A* and an observer at infinity. This allows us to calculate the approximated observed radial velocity by multiplying the two correction terms, respectively, which leads to

$$v_{\mathrm{obs}} = v_z + (1 - \gamma) + \left(1 - \sqrt{1 - \frac{r_S}{r}}\right), \qquad (2)$$

where γ is the Lorentz factor and r_S is the Schwarzschild radius.

We can then calculate a χ^2 value by comparing the model orbital motion of S2 to the observed data. For the spectral velocity measurement, the measured quantity is simply v_{obs} calculated above. For the astrometric position, the relevant quantities to compare to the GRAVITY measured separation between S2 and the emission from Sgr A* are the modelled differences in right ascension and declination $\left(\mathrm{RA}_{S2} - \mathrm{RA}_{\mathrm{Sgr\,A}^*}, \mathrm{Dec}_{S2} - \mathrm{Dec}_{\mathrm{Sgr\,A}^*}\right)$.

5.2. Posterior sampling

Once we are able to calculate a χ^2 value for any point in the parameter space, we turn to sampling methods to evaluate the posterior. Since the general three-body problem is chaotic, the orbit of S2 can depend very sensitively on the IMBH orbital parameters. If the two masses interact significantly, S2 will deviate widely from the observed orbit. This leads to a complex posterior distribution that features many local maxima and degeneracies between parameters.

We use dynamic nested sampling (Skilling 2004, 2006; Higson et al. 2019) as implemented by the dynesty code (Speagle 2020) to calculate both the posterior distribution and the model evidence. Dynamic nested sampling is a generalisation of the nested sampling algorithm, which dynamically adjusts the number of samples taken in different regions of the parameter space in order to maximise calculation accuracy. We use this approach for two principal reasons. First, nested sampling is better able to capture multi-modal posterior distributions than more traditional Markov chain Monte Carlo methods (see e.g. Ashton et al. 2022). Second, nested sampling directly calculates the evidence, allowing for model comparison (in this case between scenarios with and without an IMBH) as well as parameter constraints.

After some experimentation, we have found that a nested sampling run with at least 8000 live points is needed to reproducibly converge on the posterior distribution. We have found the best numerical performance using the 'rwalk' sampling method and the 'multi' bounding distribution (see Feroz et al. 2009; Skilling 2006, for details). In order to ensure that we have explored the full parameter space, we explored independent runs with different initialisation parameters or negligibly different boundaries as well as a run with 16 000 initial live points. We find that all produce a nearly identical posterior distribution.

To confirm the accuracy of our set-up, we compare the posterior distributions of the S2 orbital parameters as well as the mass and distance of Sgr A* with the published values. We recover the published values to within the error bars in both a fiducial run without an IMBH as well as a full run with free IMBH orbital parameters. We also recover the expected degeneracies between the mass and distance of Sgr A*.

The parameters of our simulation are summarised in Table 1. Along with the mass and the six orbital parameters of the IMBH, we allow the orbital parameters of S2, the mass and distance of Sgr A*, and a global velocity offset to vary. We chose to

Table 1. Fitting parameters, their initial values, and the boundaries.

Parameter	Starting point	Boundaries
M_0 ($M_\odot$)	4.2×10^6	$\pm 5 \times 10^5$
R_0 (kpc)	8.25	± 1.0
$v_{z,0}$ (km s^{-1})	0	± 5
a_{S2} ($''$)	0.125	± 0.02
e_{S2}	0.87	± 0.05
i_{S2} ($°$)	134	± 5
Ω_{S2} ($°$)	228	± 5
ω_{S2} ($°$)	66	± 5
$T_{peri,S2}$ (y)	2018.4	± 0.2
M_i ($M_\odot$)	5010	± 5000
a_i ($''$)	0.51	± 0.5
e_i	0.48	± 0.47
i_i ($°$)	180	± 180
Ω_i ($°$)	180	± 180
ω_i ($°$)	180	± 180
μ_i ($°$)	180	± 180

Notes. Not listed are the Sgr A* parameters ($x_0, y_0, z_0, v_{x,0}, v_{y,0}$), which are also allowed to vary.

parametrise the initial position of the S2 orbit with the time of pericentre passage T_{peri}, which is well constrained from observations. In order to limit the duplication of IMBH orbits, however, we use the mean anomaly at t_0 to parametrise its initial position, which naturally confines the initial conditions to a single orbital period.

Table 1 also shows the initial value and allowed range for each parameter. We use a flat prior across the space $(-\text{range}, +\text{range})$. The S2 orbital parameters and Sgr A* mass and distance are already tightly constrained by previous fits to (partly) the same data as used here. We adopt values close to GRAVITY Collaboration (2018), with a range scaled from the errors quoted therein. For the IMBH we allow the angular orbital parameters to vary between $0°$ and $360°$. We expect to have the greatest discriminating power for IMBHs that lie within or close to the S2 orbit, as the potential for three-body interactions is thus maximised. However, the minimum time step to accurately calculate orbits decreases as the closest approach distance decreases. This decreased time step increases the computational time for each likelihood evaluation. Given that our results depend on a robust exploration of the parameter space, we therefore choose an initial range of semi-major axes between $0.01''$ and $0.1''$ and limit eccentricities to be less than 0.95. With this set-up, a complete run of the parameter estimation can be completed on a moderately sized cluster (60 cores) within approximately one week. We additionally explore the non-hierarchical scenario in a second run where we allow the IMBH semi-major axis to extend out to $1''$.

6. Constraints on IMBHs in the GC from the S2 orbit

From the posterior sampling we obtain the full set of IMBH orbital parameters (see Appendix A). The left panel of Fig. 1 shows the posterior distribution of the IMBH mass and the

semi-major axis of its orbit for a prior range of $a_i < 0.1''$. For all IMBH semi-major axes inside the S2 orbit, we exclude IMBH masses greater than $4010\,M_\odot$ at the 86% level. At small semi-major axes $\lesssim 0.05''$, these limits are considerably stronger, and IMBHs with a mass greater than $\approx 2000\,M_\odot$ are very strongly excluded.

We find a global minimum χ^2 value of 219.53 for an IMBH with a mass of $1904\,M_\odot$ and a semi-major axis of $0.031''$, compared to a minimum χ^2 of 224.1 for an S2-only model. Since the IMBH model formally fits the data better than the S2-only model, we calculate the evidence for each model by integrating over the posterior distribution. We find that the log-evidence for the two models are essentially identical: $\log(z) = 124.80$ for S2-only, and $\log(z) = 124.79$ for the IMBH. We therefore conclude that we cannot distinguish between these models and that our constraints quoted above are indeed upper limits.

The right panel of Fig. 1 shows the posterior distribution of the IMBH mass and the semi-major axis of its orbit for a prior range of $0.1'' < a_i < 1''$. Here we find a minimum χ^2 value of 220.54 for an IMBH with a mass of $5842\,M_\odot$ and a semi-major axis of $0.164''$. However, the posterior peaks at the upper edge of the prior mass range, implying that we do not generate a valid upper limit on the mass or a constraint on the semi-major axis. These peaks in the posterior correspond to an IMBH on a large orbit that essentially does not interact with S2 over the ≈ 20-year timescale probed here, rendering it undetectable with our current method.

We find the shape of the allowed region in the $M_i - a_i$ parameter space to be roughly consistent with previous work by Gualandris et al. (2010), with the combination of high mass and small semi-major axis most strongly ruled out. However, we find higher upper mass limits than previous studies. This difference almost certainly stems from the increased sampling density of the parameter space. We find that the level of perturbation of the S2 orbit is extremely sensitive to even those parameters traditionally considered to be nuisance parameters, such as the initial mean anomaly of the orbit.

We also find a larger allowed region of the parameter space than Naoz et al. (2020). We attribute this discrepancy to the fact that the authors in that study approximate the perturbation of the S2 orbit by averaging over the orbital periods of both S2 and the IMBH. As shown in Fig. 2, the relative location of the IMBH along its orbit can play a crucial role in determining to what extent it perturbs the path of S2.

7. Constraints on IMBHs in the GC from the S-stars

In the previous section we report that certain IMBHs with specific orbital properties cannot be excluded given the current GRAVITY and SINFONI/KECK/GNIRS data of S2. In order to understand the long-term effects of such an IMBH, we place it among the 40 S-stars with known orbital parameters (see Gillessen et al. 2009, 2017) and evolve the entire system backwards in time. We essentially run the same simulation as defined in Sect. 5.1, but without the posterior sampling. The question we pose is whether the presence of an intermediate-mass perturber destabilises or even disrupts the S-stars within one million years.

We extract for each of the two scenarios 60 random IMBH orbits from within the 98.8% likelihood contours shown in Fig. 1. Then we evolve the entire system of S2, the 40 S-stars, the IMBH and Sgr A* with REBOUND/REBOUNDx for 10^6 years backwards in time. The stars are considered to be 'active particles' in the simulation (i.e. they have masses): eight early-type stars have precisely determined masses that lie between
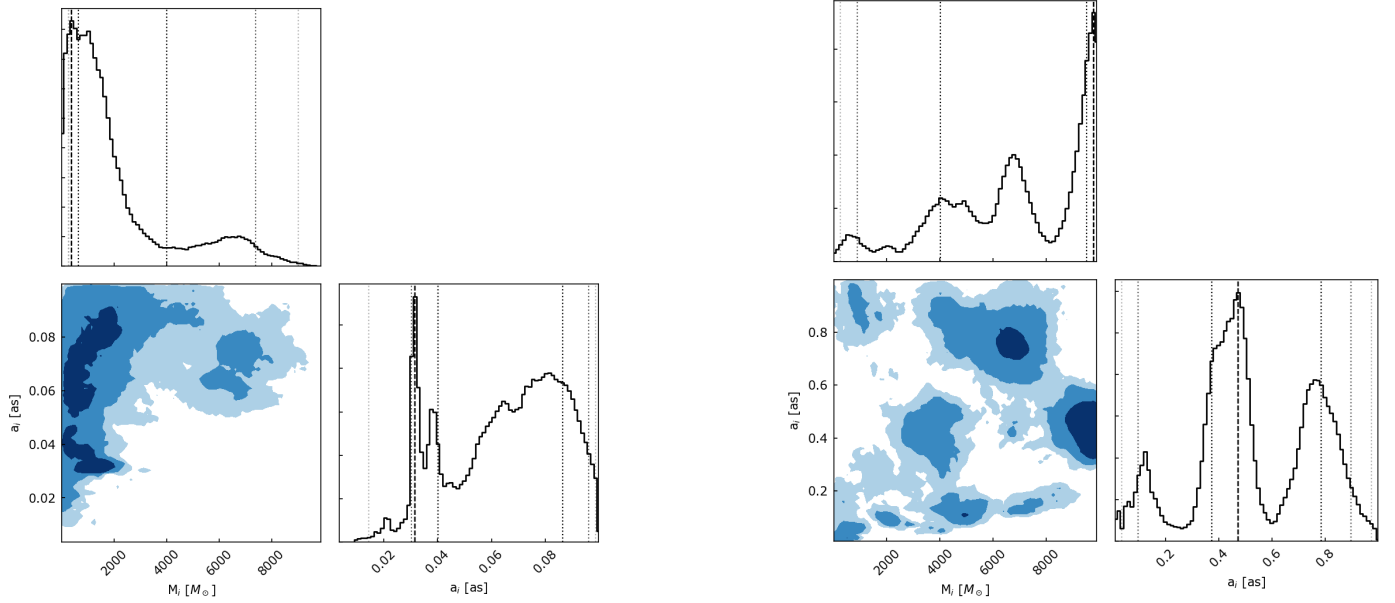
Fig. 1. Posterior distributions of IMBH orbits. Left: posterior distribution over the mass and semi-major axis of the IMBH for orbits with a semi-major axis smaller than 0.1″. The contours correspond to 39%, 86%, and 98.8% (from dark blue to light blue) enclosed likelihood. Right: same as left, but for orbits extending out to a semi-major axis of 1″.

7 and $14 \, M_\odot$ (see Habibi et al. 2017); the mass of the lesser-known early-type stars were set to $10 \, M_\odot$; the inferred mass of the population of late-type stars lies between 0.5 and $2 \, M_\odot$ (see Habibi et al. 2019), and accordingly we set the known late-type stars to $1 \, M_\odot$; as the majority of the stellar sample are early-type stars, we also assume a mass of $10 \, M_\odot$ for the two stars (S39 and S55) of unidentified spectral type.

Our criterion to define an unstable system is that within 1 Myr at least one star is ejected and moves past the stellar WR/O disc to reach a separation $r > 3000″$ (about 120 pc) from Sgr A*. At this distance the stars are far outside the sphere of influence, which has for Sgr A* a radius of about 3 pc, and appear completely dissociated from the S-star cluster. Depending on the strength of interaction with the IMBH, some of the ejected stars may return to Sgr A* after increasingly long intervals of time (and on severely modified orbits) which are, however, not covered by our simulation.

We find that all of our IMBH solutions introduce some degree of instability among the S-stars such that their orbits deviate substantially from the non-IMBH case. Furthermore, the majority of our IMBH solutions fulfil our instability criterion: at least one star (but typically several stars) becomes unbound and is ejected well before one million years have passed. The S-stars that strongly interact with an IMBH are in particular the highly eccentric stars such as S9, S14, and S29 with $e > 0.9$. Only a small fraction of about 5% and 1.6% of the inner and outer IMBH solutions, respectively, does not disrupt the S-stars in 1 Myr. The stability of the S-star cluster thus gives a more stringent constraint than the best-fitting S2 orbit alone.

In our sample of 60 inner IMBH configurations, the only three non-disruptive inner solutions for semi-major axes $0.01″ < a_i < 0.1″$ (labelled $IMBH_{i1}$, $IMBH_{i2}$, $IMBH_{i3}$) have similar orbital parameters: masses below $2000 \, M_\odot$, moderate to high eccentricities, and a significant inclination towards the S2-plane of at least 60°. We show their orbital properties together with the only non-disruptive outer solution ($IMBH_{o1}$) in Table 2. Interestingly, the only valid outer solution we find has a mass and semi-major axis that falls into the parameter range proposed by
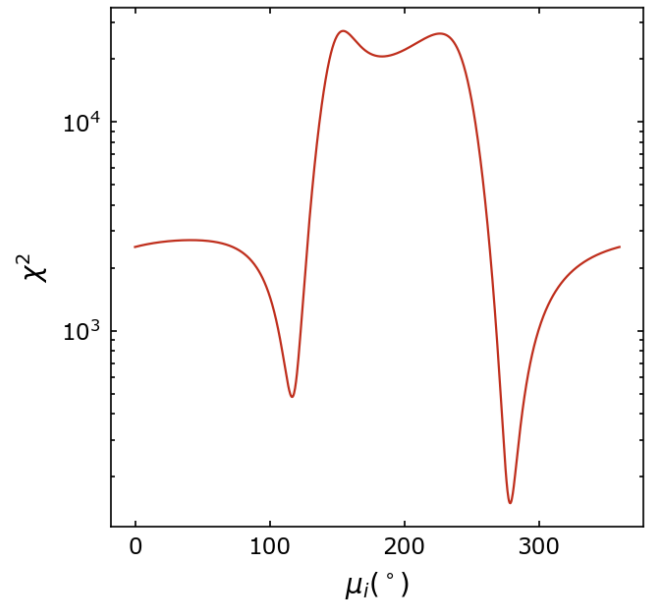
Merritt et al. (2009; i.e. at first glance an IMBH that could potentially thermalise the S-stars in a sufficiently short time).

The three stable inner IMBH orbits are shown in Fig. 3. We note that we have included the adaptive optics positions measured with the NACO instrument in the plot, although these data points were not used for fitting. The three IMBH orbits shown in blue correspond to the IMBH orbital properties given in Table 2 and their residuals are given in Fig. B.1. They demonstrate where and how an IMBH could hide in the GC based on the current GRAVITY and SINFONI/KECK/GNIRS data: the IMBH must have a rather low mass and be on a short orbit around Sgr A* that is sufficiently inclined towards the orbital plane of S2.
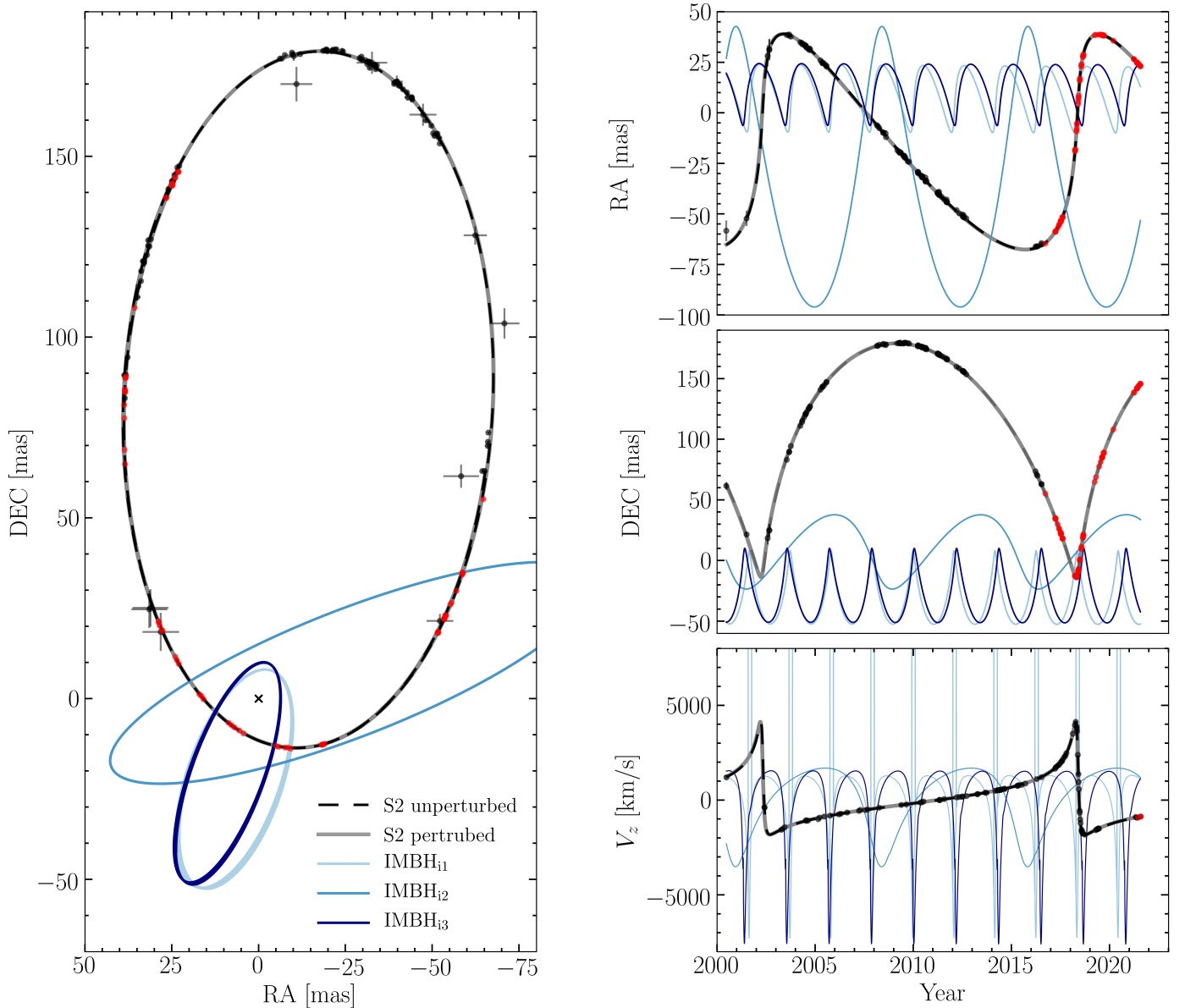

Fig. 2. χ^2 vs. the initial mean anomaly of the IMBH. All other IMBH parameters are fixed to the values shown in Table 2 and used in Fig. 3.

Fig. 3. Example orbits of allowed IMBHs in the Galactic Centre. The left panel shows the on-sky orbits of S2 and three IMBH solutions around Sgr A* (indicated by the cross). The right panels show the time evolution of the RA, Dec, and radial velocity. The solid grey and dashed black curves show the orbit of S2 with and without an IMBH, respectively. The IMBHs are shown in blue and correspond to the parameters given in Table 2. The data points show the last 30 years of observations of S2. The black points correspond to adaptive optics measurements with NACO and early speckle imagery with SHARP. The red points correspond to GRAVITY interferometric measurements. The black and red radial velocity observations correspond, respectively, to SINFONI – KECK and GNIRS spectral measurements of the line-of-sight velocity.

Table 2. Example solutions of allowed IMBH parameters that do not disrupt the S-star cluster in 1 Myr.

Parameter	$IMBH_{i1}$	$IMBH_{i2}$	$IMBH_{i3}$	$IMBH_{o1}$
M_i ($M_\odot$)	1282	1321	1130	3226
a_i ($''$)	0.032	0.033	0.075	0.435
e_i	0.73	0.69	0.49	0.56
i_i (°)	52.29	63.85	75.31	274.03
Ω_i (°)	155.42	161.59	291.45	95.95
ω_i (°)	195.74	171.54	156.02	180.71

Notes. The $IMBH_{i1}$–$IMBH_{i3}$ solutions lie inside the S2 orbit, while $IMBH_{o1}$ is outside.

8. Discussion

Intermediate-mass black holes are thought to play a vital role in the growth of massive and supermassive BHs. They are thus closely linked to the formation and evolution of their host galaxies and are predicted to be abundant in the local universe (e.g. in young dense stellar clusters and dwarf galaxies). However, IMBHs are notoriously difficult to find and unambiguously identify[4]. The presence or absence of an IMBH in the centre of the Milky Way could give important hints to constrain their

---

[4] Most IMBHs are thought to roam about alone and rarely accrete matter. Candidate IMBHs are almost exclusively found indirectly as the gravitational source of hyper-velocity compact clouds and hyper-velocity stars, irregular stellar and pulsar dynamics, or in transient ultra-luminous X-ray sources.

formation channel and provide valuable input for future electromagnetic and gravitational wave observations with the Extremely Large Telescope (ELT, e.g. Davies et al. 2018) and the Laser Interferometer Space Antenna (LISA, planned launch date in 2037; see e.g. Amaro-Seoane et al. 2017), respectively.

In this paper we used the high angular resolution astrometric and spectroscopic data of the star S2 from GRAVITY and SINFONI/KECK/GNIRS, respectively, to assess where in the GC an IMBH could hide. We had a fresh look at the dynamical search for IMBHs in the GC by exploring the full 16-dimensional parameter space of the chaotic three-body problem comprising Sgr A*, an IMBH, and the star S2. We specifically considered two scenarios, one where the IMBH trajectory lies inside the S2 orbit with a semi-major axis $0.01'' < a_i < 0.1''$ and the other where the IMBH trajectory crosses the S2 orbit or lies outside, $0.1'' < a_i < 1''$, and calculated for both cases the resulting modified orbital properties for S2. Using dynamic nested sampling, we explored the full set of parameters and found for each scenario the most likely locations for an IMBH (see Fig. 1).

We found that for very specific combinations of orbital parameters, in particular for certain IMBH orientations and pericentre passage times, high IMBH masses could be located among the S-stars. This happens for IMBHs that stay sufficiently far from S2 during their closest approach to Sgr A* so as not to measurably affect the orbit at all. We therefore analysed our valid solutions further and selected for each scenario 60 random solutions from within the 98.8% likelihood contours (see Fig. 1). These IMBHs were placed among the 40 stars of the S-star cluster and evolved backwards in time for one million years. Moreover, we calculated for each set of 60 solutions the residuals between the data and the models.

Based on the results from the optimisation, the stability analysis and the residual calculation, we arrive at the conclusion that although we find viable fits to the data that suggest an IMBH could be present for specific parameter combinations, the majority of these solutions do not withstand the reality check and would disrupt the S-star cluster in less than a million years or induce a precession in the orbit of S2 beyond the observed one. We conclude the following:

– Current GRAVITY and SINFONI/KECK/GNIRS data do not formally require the presence of an IMBH.
– IMBHs on orbits that cross the S2 orbit or lie outside the S2 orbit among the other S-stars are disfavoured as they typically disrupt the S-star cluster in less than one million years (only 1.6% of the solutions with $0.1'' < a_i < 1''$ are stable).
– A low-mass IMBH with $M < 2000\,M_\odot$ could hide inside the S2 orbit if its orbit is sufficiently inclined towards S2 (only 5% of the solutions with $0.01'' < a_i < 0.1''$ are stable, all of them low-mass IMBHs).

We conclude the following from the IMBH constraints on the population(s) of stars and stellar remnants in the GC: A spherical distribution of stellar-mass BHs, neutron stars (NSs) and/or white dwarfs (WDs) located as a dark cluster among the S-stars would be affected by an IMBH in a very similar way to the S-stars. The bodies on eccentric orbits would most likely be ejected, leaving preferentially the compact objects on low-eccentricity orbits behind. The total mass of such a dark (extended) cluster has been constrained to about $15\,000\,M_\odot$ within the S-star cluster. Conversely, in the absence of an IMBH among the S-stars, which is based on our analysis the preferred case, a dark cluster of SBHs, NSs, and/or WDs could show a wide range of eccentricities and orbital inclinations, and thus exhibit morphological similarities to the S-star cluster.

The high-precision GRAVITY astrometric measurements span at present about half of the S2 orbit. Much stronger constraints on the properties of IMBHs can be obtained once GRAVITY has measured a full S2 orbit. Already the current SINFONI/KECK/GNIRS data which cover, albeit sparsely, the 2002 pericentre passage hint that two consecutive pericentre passages will be invaluable to assess the likelihood of a low-mass IMBH on a <0.1'' orbit. After the upcoming closest approach of S2 to Sgr A* in 2034, the data will allow us to put stronger constraints on a single IMBH companion of Sgr A* as well as its extended mass (see GRAVITY Collaboration 2022; Heißel et al. 2022; Rubilar & Eckart 2001). Moreover, there are now several other stars with complete or near-complete orbits that can already serve in the coming few years as additional precision probes. Knowing whether or not the nuclear cluster in the GC hosts an IMBH will in turn put constraints on the formation processes of IMBHs. Moreover, constraints on the mass distribution in the GC will also be of value to LISA, which will be able to measure gravitational waves of moving masses in the GC.

References

Abbott, R., Abbott, T. D., Abraham, S., et al. 2020a, Phys. Rev. Lett., 125, 101102
Abbott, R., Abbott, T. D., Abraham, S., et al. 2020b, ApJ, 900, L13
Abbott, R., Abbott, T. D., Abraham, S., et al. 2021, Phys. Rev. X, 11, 021053
Alexander, T., & Hopman, C. 2009, ApJ, 697, 1861
Amaro-Seoane, P., Konstantinidis, S., Dewi Freitag, M., Miller, M. C., & Rasio, F. A. 2014, ApJ, 782, 97
Amaro-Seoane, P., Audley, H., Babak, S., et al. 2017, ArXiv e-prints [arXiv:1702.00786]
Amorim, A., Bauböck, M., Berger, J. P., et al. 2019, Phys. Rev. Lett., 122, 101102
Antonini, F., Gieles, M., & Gualandris, A. 2019, MNRAS, 486, 5008
Ashton, G., Bernstein, N., Buchner, J., et al. 2022, Nat. Rev. Meth. Primers, 2
Bañados, E., Venemans, B. P., Mazzucchelli, C., et al. 2018, Nature, 553, 473
Bartko, H., Martins, F., Fritz, T. K., et al. 2009, ApJ, 697, 1741
Bartko, H., Martins, F., Trippe, S., et al. 2010, ApJ, 708, 834
Baumgardt, H., Makino, J., & Hut, P. 2005, ApJ, 620, 238
Becklin, E. E., & Neugebauer, G. 1968, ApJ, 151, 145
Begelman, M. C. 2010, MNRAS, 402, 673
Begelman, M. C., Volonteri, M., & Rees, M. J. 2006, MNRAS, 370, 289
Bustamante-Rosell, M. J., Noyola, E., Gebhardt, K., et al. 2021, ApJ, 921, 107
Casares, J., & Jonker, P. G. 2014, Space Sci. Rev., 183, 223
Chen, X., & Amaro-Seoane, P. 2014, ApJ, 786, L14
Chen, X., & Amaro-Seoane, P. 2015, Class. Quant. Grav., 32, 064001
Corral-Santana, J. M., Casares, J., Muñoz-Darias, T., et al. 2016, A&A, 587, A61

Davies, R., Alves, J., Clénet, Y., et al. 2018, in Ground-based and Airborne Instrumentation for Astronomy VII, eds. C. J. Evans, L. Simard, & H. Takami, SPIE Conf. Ser., 10702, 107021S
Do, T., Hees, A., Ghez, A., et al. 2019, Science, 365, 664
Eckart, A., & Genzel, R. 1996, Nature, 383, 415
Eisenhauer, F., Genzel, R., Alexander, T., et al. 2005, ApJ, 628, 246
Erkal, D., Boubert, D., Gualandris, A., Evans, N. W., & Antonini, F. 2019, MNRAS, 483, 2007
Farrell, S. A., Webb, N. A., Barret, D., Godet, O., & Rodrigues, J. M. 2009, Nature, 460, 73
Feldmeier-Krause, A., Neumayer, N., Schödel, R., et al. 2015, A&A, 584, A2
Feroz, F., Hobson, M. P., & Bridges, M. 2009, MNRAS, 398, 1601
Fragione, G., Kocsis, B., Rasio, F. A., & Silk, J. 2022, ApJ, 927, 231
Freitag, M., Gürkan, M. A., & Rasio, F. A. 2006, MNRAS, 368, 141
Fritz, T. K., Chatzopoulos, S., Gerhard, O., et al. 2016, ApJ, 821, 44
Generozov, A., & Madigan, A.-M. 2020, ApJ, 896, 137
Ghez, A. M., Klein, B. L., Morris, M., & Becklin, E. E. 1998, ApJ, 509, 678
Ghez, A. M., Duchêne, G., Matthews, K., et al. 2003, ApJ, 586, L127
Ghez, A. M., Salim, S., Weinberg, N. N., et al. 2008, ApJ, 689, 1044
Gillessen, S., Eisenhauer, F., Trippe, S., et al. 2009, ApJ, 692, 1075
Gillessen, S., Plewa, P. M., Eisenhauer, F., et al. 2017, ApJ, 837, 30
GRAVITY Collaboration (Abuter, R., et al.) 2018, A&A, 615, L15
GRAVITY Collaboration (Abuter, R., et al.) 2019, A&A, 615, L10
GRAVITY Collaboration (Abuter, R., et al.) 2020, A&A, 636, L5
GRAVITY Collaboration (Abuter, R., et al.) 2021, A&A, 647, A59
GRAVITY Collaboration (Abuter, R., et al.) 2022, A&A, 657, L12
Greene, J. E., Strader, J., & Ho, L. C. 2020, ARA&A, 58, 257
Gualandris, A., & Merritt, D. 2009, ApJ, 705, 361
Gualandris, A., Gillessen, S., & Merritt, D. 2010, MNRAS, 409, 1146
Habibi, M., Gillessen, S., Martins, F., et al. 2017, ApJ, 847, 120
Habibi, M., Gillessen, S., Pfuhl, O., et al. 2019, ApJ, 872, L15
Hailey, C. J., Mori, K., Bauer, F. E., et al. 2018, Nature, 556, 70
Hansen, B. M. S., & Milosavljević, M. 2003, ApJ, 593, L77
Heißel, G., Paumard, T., Perrin, G., & Vincent, F. 2022, A&A, 660, A13
Higson, E., Handley, W., Hobson, M., & Lasenby, A. 2019, Stat. Comput., 29, 891
Hills, J. G. 1988, Nature, 331, 687
Hoyle, F., & Fowler, W. A. 1963, Nature, 197, 533
Kormendy, J., & Ho, L. C. 2013, ARA&A, 51, 511
Loeb, A., & Rasio, F. A. 1994, ApJ, 432, 52
Lu, J. R., Ghez, A. M., Hornstein, S. D., et al. 2009, ApJ, 690, 1463
Lu, J. R., Do, T., Ghez, A. M., et al. 2013, ApJ, 764, 155
Madau, P., & Rees, M. J. 2001, ApJ, 551, L27
Magorrian, J., Tremaine, S., Richstone, D., et al. 1998, AJ, 115, 2285
Merritt, D., Gualandris, A., & Mikkola, S. 2009, ApJ, 693, L35
Mezcua, M. 2017, Int. J. Mod. Phys. D, 26, 1730021
Mezcua, M., Civano, F., Fabbiano, G., Miyaji, T., & Marchesi, S. 2016, ApJ, 817, 20
Mezcua, M., Civano, F., Marchesi, S., et al. 2018, MNRAS, 478, 2576
Miller, M. C., & Colbert, E. J. M. 2004, Int. J. Mod. Phys. D, 13, 1
Miller, M. C., & Hamilton, D. P. 2002, MNRAS, 330, 232
Miller, M. C., & Lauburg, V. M. 2009, ApJ, 692, 917
Mirabel, F. 2017, New Astron. Rev., 78, 1
Mortlock, D. J., Warren, S. J., Venemans, B. P., et al. 2011, Nature, 474, 616
Naoz, S., Will, C. M., Ramirez-Ruiz, E., et al. 2020, ApJ, 888, L8
Narayan, R., & McClintock, J. E. 2013, ArXiv e-prints [arXiv:1312.6698]
Neumayer, N., Seth, A., & Böker, T. 2020, A&ARv, 28, 4
Nitz, A. H., & Capano, C. D. 2021, ApJ, 907, L9
Ohkubo, T., Nomoto, K., Umeda, H., Yoshida, N., & Tsuruta, S. 2009, ApJ, 706, 1184
Oppenheimer, J. R., & Snyder, H. 1939, Phys. Rev., 56, 455
Paumard, T., Genzel, R., Martins, F., et al. 2006, ApJ, 643, 1011
Penrose, R. 1965, Phys. Rev. Lett., 14, 57
Perets, H. B., Gualandris, A., Kupi, G., Merritt, D., & Alexander, T. 2009, ApJ, 702, 884
Pfuhl, O., Fritz, T. K., Zilka, M., et al. 2011, ApJ, 741, 108
Portegies Zwart, S. F., & McMillan, S. L. W. 2002, ApJ, 576, 899
Quinlan, G. D., & Shapiro, S. L. 1990, ApJ, 356, 483
Rashkov, V., & Madau, P. 2014, ApJ, 780, 187
Rees, M. J. 1978, The Observatory, 98, 210
Reid, M. J., & Brunthaler, A. 2004, ApJ, 616, 872
Reid, M. J., & Brunthaler, A. 2020, ApJ, 892, 39
Rein, H., & Liu, S. F. 2012, A&A, 537, A128
Rein, H., & Spiegel, D. S. 2015, MNRAS, 446, 1424
Rizzuto, F. P., Naab, T., Spurzem, R., et al. 2021, MNRAS, 501, 5257
Rose, S. C., Naoz, S., Sari, R., & Linial, I. 2022, ApJ, 929, L22
Rubilar, G. F., & Eckart, A. 2001, A&A, 374, 95
Schödel, R., Ott, T., Genzel, R., et al. 2002, Nature, 419, 694
Schödel, R., Feldmeier, A., Kunneriath, D., et al. 2014, A&A, 566, A47
Skilling, J. 2004, in Bayesian Inference and Maximum Entropy Methods in Science and Engineering: 24th International Workshop on Bayesian Inference and Maximum Entropy Methods in Science and Engineering, eds. R. Fischer, R. Preuss, & U. V. Toussaint, AIP Conf. Ser., 735, 395
Skilling, J. 2006, Bayesian Anal., 1, 833
Soltan, A. 1982, MNRAS, 200, 115
Speagle, J. S. 2020, MNRAS, 493, 3132
Stone, N. C., Küpper, A. H. W., & Ostriker, J. P. 2017, MNRAS, 467, 4180
Tamayo, D., Rein, H., Shi, P., & Hernandez, D. M. 2020, MNRAS, 491, 2885
Tep, K., Fouvry, J.-B., Pichon, C., et al. 2021, MNRAS, 506, 4289
Volonteri, M. 2010, A&ARv, 18, 279
von Fellenberg, S. D., Gillessen, S., Stadler, J., et al. 2022, ApJ, 932, L6
Webb, N. A., Guérou, A., Ciambur, B., et al. 2017, A&A, 602, A103
Wise, J. H., Regan, J. A., O'Shea, B. W., et al. 2019, Nature, 566, 85
Wu, X.-B., Wang, F., Fan, X., et al. 2015, Nature, 518, 512
Yang, J., Wang, F., Fan, X., et al. 2020, ApJ, 897, L14
Yelda, S., Ghez, A. M., Lu, J. R., et al. 2014, ApJ, 783, 131
Yu, Q., & Tremaine, S. 2003, ApJ, 599, 1129

1 Max Planck Institute for Extraterrestrial Physics, Giessenbachstraße 1, 85748 Garching, Germany
  e-mail: ostraub@mpe.mpg.de
2 ORIGINS Excellence Cluster, Boltzmannstraße 2, 85748 Garching, Germany
3 Department of Physics, University of Illinois, 1110 West Green Street, Urbana, IL 61801, USA
4 European Southern Observatory, Karl-Schwarzschild-Straße 2, 85748 Garching, Germany
5 LESIA, Observatoire de Paris, Université PSL, CNRS, Sorbonne Université, Université de Paris, 5 place Jules Janssen, 92195 Meudon, France
6 Universidade de Lisboa – Faculdade de Ciências, Campo Grande, 1749-016 Lisboa, Portugal
7 CENTRA – Centro de Astrofísica e Gravitação, IST, Universidade de Lisboa, 1049-001 Lisboa, Portugal
8 Univ. Grenoble Alpes, CNRS, IPAG, 38000 Grenoble, France
9 Max Planck Institute for Astronomy, Königstuhl 17, 69117 Heidelberg, Germany
10 Universidade do Porto, Faculdade de Engenharia, Rua Dr. Roberto Frias, 4200-465 Porto, Portugal
11 Department of Astrophysical & Planetary Sciences, JILA, University of Colorado, Duane Physics Bldg., 2000 Colorado Ave, Boulder, CO 80309, USA
12 Faculdade de Engenharia, Universidade do Porto, Rua Dr. Roberto Frias, 4200-465 Porto, Portugal
13 Hamburger Sternwarte, Universität Hamburg, Gojenbergsweg 112, 21029 Hamburg, Germany
14 Departments of Physics and Astronomy, Le Conte Hall, University of California, Berkeley, CA 94720, USA
15 European Southern Observatory, Casilla 19001, Santiago 19, Chile
16 Max Planck Institute for Astrophysics, Karl-Schwarzschild-Straße 1, 85748 Garching, Germany
17 Institute of Physics, University of Cologne, Zülpicher Straße 77, 50937 Cologne, Germany
18 Max Planck Institute for Radio Astronomy, Auf dem Hügel 69, 53121 Bonn, Germany
19 Institute of Multidisciplinary Mathematics, UPV, Camino de Vera, s/n 46022 Valencia, Spain
20 Kavli Institute for Astronomy and Astrophysics, Peking University, 5 Yiheyuan Rd, Haidian, Beijing 100871, PR China
21 Advanced Concepts Team, European Space Agency, TEC-SF, ESTEC, Keplerlaan 1, 2201 AZ Noordwijk, The Netherlands
22 Niels Bohr International Academy, Niels Bohr Institute, Blegdamsvej 17, 2100 Copenhagen, Denmark

Appendix A: The full IMBH parameter space

Figure A.1 shows the posterior over all of the IMBH orbital parameters. For clarity in plotting, we do not show the param-eters of the S2 orbit, which are also allowed to vary over the fit. We find that the S2 parameters are tightly constrained and that their values match those found in previous works (e.g. GRAVITY Collaboration 2018).
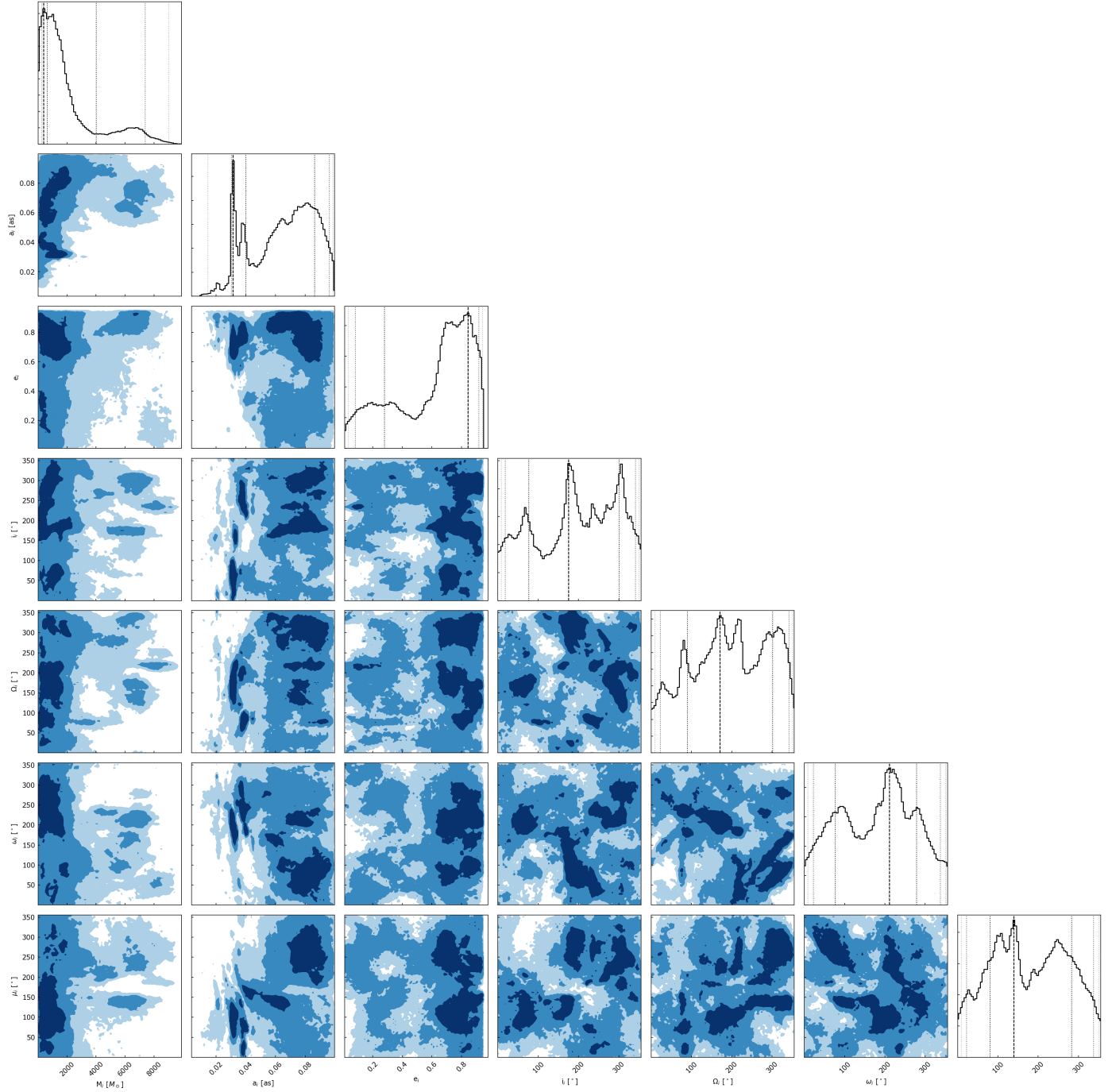

Fig. A.1. Corner plot of the posterior of the IMBH orbital parameters for the hierarchical case. Not shown are the parameters of the S2 orbit, which are also allowed to vary.

Appendix B: Residuals

We calculate the residuals between the S2 data and the model orbits for all 60 inner and outer IMBH solutions. Figure B.1 compares the astrometry residuals of the unperturbed Schwarzschild orbit (black markers) of S2 to the three orbits that are modified by an inner IMBH (blue dots) and the orbit modified by an outer IMBH (green diamonds). The entirety of all residuals, including orbits that have been rejected based on stability arguments, are shown as a open symbols in the background. Both the inner and the outer stable IMBH solutions have residuals comparable to a pure Schwarzschild orbit.
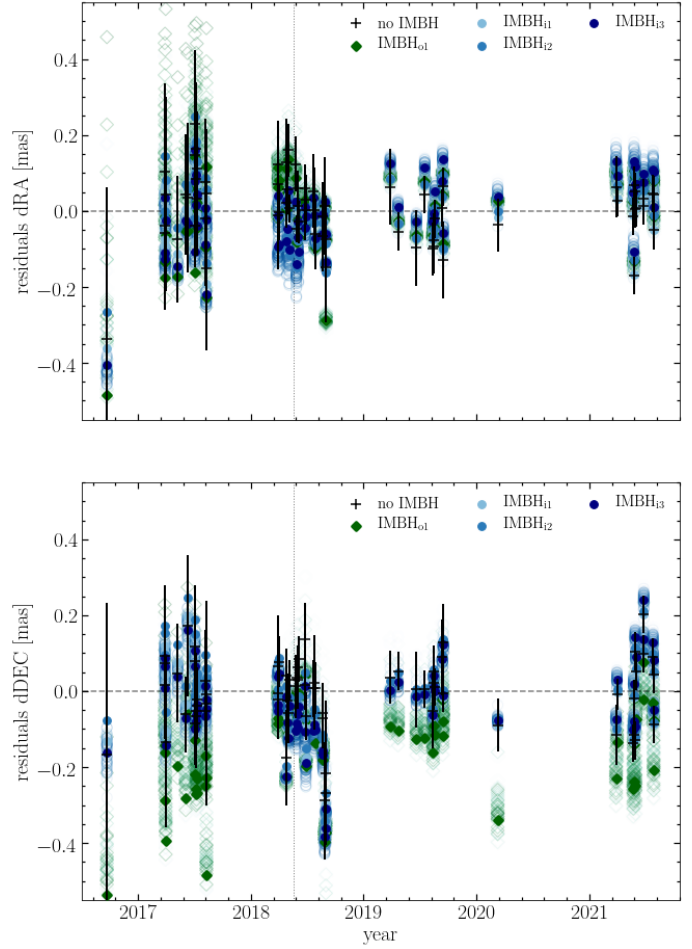

Fig. B.1. Residuals of the S2 orbit. The best-fitting Schwarzschild model (i.e. without the presence of an IMBH) is marked in black. The blue open circles denote the 60 solutions where the IMBH orbit lies inside the S2 orbit, $0.01'' < a_i < 0.1''$, and the green open diamonds are the 60 outer IMBH solutions with $0.1'' < a_i < 1''$. The filled symbols highlight solutions shown in Table 2. The fine vertical line indicates the time of pericentre passage. Upper panel: Data–model difference for the right ascension (dRA). Bottom panel: Data–model difference for the declination (dDEC).